AIAA 2002-3663

A Non-Equilibrium Numerical Study of a Microwave Electrothermal Thruster

V. P. Chiravalle R. B. Miles and E. Y. Choueiri
Princeton University
Princeton, NJ, 08544

38th AIAA Joint Propulsion Conference
July 7–10, 2002/Indianapolis, IN

A Non-Equilibrium Numerical Study of a Microwave Electrothermal Thruster

V. P. Chiravalle * R. B. Miles † and E. Y. Choueiri ‡
Princeton University
Princeton, NJ, 08544

A numerical simulation of a microwave electrothermal thruster, incorporating two-temperature, non-equilibrium effects, is presented. This model includes the complete system of both the Maxwell equations and the Navier-Stokes equations for the case of a helium flow with different electron and heavy species temperatures, with finite rate ionization and excitation kinetics including 12 electron-impact reactions and Penning ionization, with routines for calculating transport properties of heavy particles and electrons using kinetic theory, and with a finite-element solver for calculating heat transfer through the nozzle. Results from a simulation of the thruster are presented, involving a 220 mg/sec helium flow, with 4 kW of energy addition in the plenum section. This model is shown to give predictions of both the peak electron temperature (15,100 K) and the radial electron temperature profile, which are closer to the available data, than previous equilibrium models.

Introduction

A microwave electrothermal thruster is a space propulsion system that uses a microwave plasma to heat a low molecular weight propellant gas to a high temperature, and like in a conventional rocket engine the propellant gas then expands isentropically in a nozzle to produce thrust. Unlike other electrothermal propulsion systems, such as resistojets and arcjets,[1] microwave thrusters have not been used on spacecraft. A state-of-the-art, 2 kW hydrazine arcjet has demonstrated a specific impulse of roughly 600 sec and an efficiency of 30 % during a 550-h test.[2] The fact that a microwave-sustained plasma can be created without electrodes and can be maintained away from the material surfaces of the thruster, may allow for large reductions in thruster erosion and significant improvements in overall lifetime, compared with arcjets. Experiments with early microwave thruster prototypes have shown that the microwave-sustained plasma becomes unstable above a certain threshold of absorbed power, and this threshold is a function of mass flow rate and plenum pressure.[3] Since microwave thrusters are inherently two-dimensional in nature, and a plethora of electron-driven processes contribute to the formation and maintenance of a microwave-sustained plasma, when addressing this problem from a theoretical point of view it is necessary to solve the complete set of fluid conservation equations in order to understand the heating process. Furthermore, it is the belief of the authors that non-equilibrium effects, in particular the disparity between the heavy particle and electron temperatures, are critical in being able to predict the heating process in microwave thrusters and the instabilities associated with it, and therefore we have created a non-equilibrium model to address this need.

Previous Work

Different configurations have been explored for coupling microwave power to a gas, the most promising for thruster applications is the cylindrical resonant cavity design, employing either the TM_{011} or TM_{012} microwave mode structure. The first thruster of this kind was built in the early 1980's and it consisted of a cylindrical microwave resonant cavity at 2.45 GHz and a quartz tube, arranged concentrically.[4] He or N_2 gas flowed

*Graduate Student, Mechanical & Aerospace Engineering
†Professor, Mechanical & Aerospace Engineering
‡Chief Scientist at EPPDyL. Professor, Mechanical & Aerospace Engineering

Presented as Paper 2002–3663 at the AIAA 38th Joint Propulsion Conference, Indianapolis, IN, July 7–10 2002

through the quartz tube, where the walls stabilized the microwave plasma on the centerline. The gas then exited through a quartz nozzle connected to the tube. Another prototype thruster utilizing a cylindrical resonant cavity at 2.45 Ghz with a free-floating plasma inside the cavity has operated successfully at power levels of up to 2.2 kW and pressures as high as 3 atm with He, N_2, NH_3 and H_2 as propellants.[5] In that design the plasma is stabilized by flow swirl created from tangential gas injection into the cavity. The gas exits the cavity through a graphite nozzle.

In addition to these experimental efforts, numerical work has been done to model the physical processes occurring in microwave-sustained discharges. The size, shape, location and peak temperature of the free-floating He discharges, stabilized by a bluff body, discussed above have been reasonably well predicted by a computational model consisting of a low Mach number formulation of the Navier-Stokes and the Maxwell equations.[6] Thermodynamic equilibrium was assumed, in the sense that both electrons and heavy species have the same temperature and that the electron concentration is determined from the Saha relation. Subsequently, the model was extended to include a converging-diverging nozzle section so that realistic thruster configurations could be simulated, and a parametric study of the effect of nozzle throat area, discharge pressure and absorbed power on the location of the plasma in a resonant cavity thruster was performed.[7] Numerical models including the effects of distinct electron and heavy species temperatures have been developed and used to simulate arcjets,[8,9] and MPD thrusters.[10,11]

Recently the authors developed such a model to simulate the supersonic stage of a two-stage microwave thruster.[12] In this work we improve this model by adding additional physics and apply it to simulate a standard microwave elctrothermal thruster, for which some experimental data exists, as a first step before simulating the entire two-stage thruster. In comparison with earlier results for energy addition to supersonic argon flows, using a single-temperature equilibrium model,[13] it was shown that with the two-temperature non-equilibrium model the electron number density is more evenly distributed throughout the flow field, as opposed to being sharply concentrated in one location, as was the case with the single-temperature model.

In this paper we simulate the flow in a standard microwave thruster (i.e. with subsonic energy addition only), but using a configuration for which a second stage can be added in the future. As a result of plasma instabilities the maximum temperature in the standard microwave thruster, and hence the specific impulse, is limited. One possible way to circumvent this limitation and to realize higher performance in terms of specific impulse and thrust is to add additional energy to the propellant in the supersonic region of the flow, using a second microwave cavity. The simulation of the full two-stage thruster will be the subject of a future paper. The model presented here is an extension of the previous model,[12] with the addition of several new and essential elements. These include a structured grid, with grid points arranged to fill completely the complex geometry of the prototype thruster, electronically excited species including the helium metastables and molecular ions, a full set of excitation and ionization rate cofficients, including the effects of electron impact processes and Penning ionization, routines for calculating the tranport properties of heavy particles and electrons, using kinetic theory and semi-empirical mixture rules, and a finite element solver for computing the heat transfer at the nozzle wall.

Outline

The physical model and the numerical techniques used in the present study are discussed briefly in the next section. The simulation results are presented following the description of the physical model. These results are compared with previous work and an outline of necessary future work is given in the conclusions section.

Physical Model

The physical model used in this work shares many features with a previous, but less physically inclusive model, developed by the authors to study supersonic helium plasmas.[12] The microwave field in the cylindrical waveguide, which forms the plenum of the thruster where subsonic energy addition takes place, is solved using essentially the same finite-element code as in previous work.[12,13] This code finds the axial and radial components of the complex electric field, with

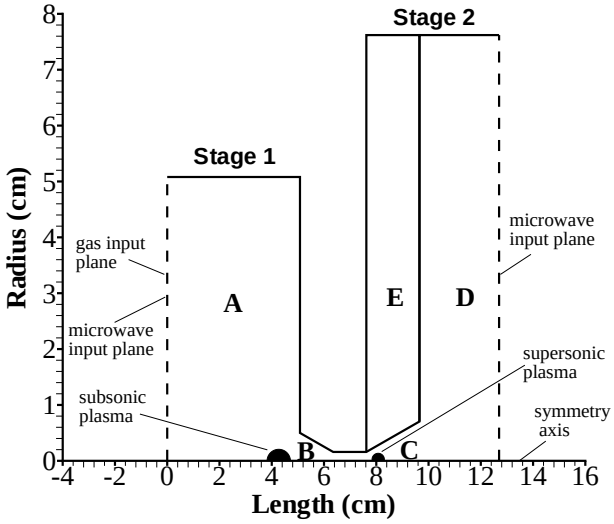

Fig. 1 The geometry used to simulate the microwave thruster. The subsonic plenum is labeled as A, the converging nozzle as B, the diverging nozzle as C, the vacuum expansion section as D and the dielectric nozzle wall as E.

each field component described by the Helmholtz equation. The fluid model incorporates the same Navier-Stokes solver as well, with additional equations for the densities of the helium ground state, of four electronically excited states consisting of the two helium metasable states and two additional excited levels, and of helium ions and molecular ions. According to the LS coupling rules, the helium atom can be divided into two sets of excited states, singlet and triplet states. The ground state of helium is a singlet state and we denote it as $1\ ^1S$. The two helium metastable states are denoted $2\ ^1S$ and $2\ ^3S$, for the singlet and triplet states respectively. The two additional excited states which are considered are the $2\ ^1P$ and the $2\ ^3P$ states. Helium ions are labeled as He^+, and helium molecular ions are labeled as He_2^+.

Flowfield Configuration

Our simulation was made for the case of helium propellant because existing electron temperature data[14] offers a good basis for comparison. A practical electrothermal thruster would use a storable space propellant such as hydrazine, ammonia or water. The geometry of the two-stage microwave thruster considered in this paper is illustrated in Fig. 1. The thruster consists of two cylindrical waveguides sections, one waveguide which brings microwave energy for the subsonic plasma, labeled Stage 1 in Fig. 1, and another which brings microwave energy for the supersonic plasma, labeled Stage 2. Stage 1 has a radius of 5.08 cm and Stage 2 has a radius of 7.63 cm. These values, and all the other dimensions to follow, were chosen to match closely a prototype two-stage thruster which has been built. In this ideal representation, microwave energy can enter each of the waveguides separately, through one of the planes indicated by a dashed line in Fig. 1, and both of the waveguides are terminated by a perfectly conducting plate. Only subsonic energy addition is considered in this study, and so Stage 2 is not discussed further. The complex electric field is specified at the microwave input plane of Stage 1, using a theoretical expression for a cylindrical, TM_{01} mode with the amplitude chosen so that the desired amount of power is absorbed by the subsonic plasma.

The propellant gas, helium, enters the plenum, section A, at $x = 0$ in Fig. 1, and is subsequently heated by a microwave-sustained plasma in Stage 1: this heating process and the properties of the microwave-sustained plasma are the focus of this paper. At the inlet it is assumed that the heavy particle and electron temperatures are 500 K, the total gas pressure is 1 atm, and the concentrations of excited species and ions are given by the corresponding equilibrium values for a 6000 K plasma. This specification of species densities at the inlet boundary was made so that when the calculation begins there is a sufficient level of electrons in the plenum to couple effectively to the microwave field. The flow moves through the plenum section into a converging conical nozzle, section B, which connects to a throat region with a radius of 1.59 mm. The supersonic energy addition section is labeled as section C and it is a diverging conical nozzle with a half angle of 15 degrees and a length of 2.03 cm. The flow then exits the thruster into a vacuum expansion region, labeled as section D. The diverging part of the nozzle, labeled as section E in the diagram, is made of alumina ceramic and the subsonic part of the nozzle, corresponding to section B, is made of steel. For the purposes of calculating the heat transfer rates at the nozzle wall boundary, using the finite-element solver described later, the thermal conductivities of alumina and steel are taken to be 10 and 50 W/mK

respectively.[15] Alumina was chosen for the supersonic nozzle section because it has a low dielectric loss tangent, and thus microwaves can propagate through it with relatively little attenuation, enabling supersonic energy addition to take place, although we do not look at a case with supersonic energy addition in this paper. The fluid properties in sections A,B,C and D are determined by solving the Navier-Stokes equations, with the conditions specified above in the plenum section, and assuming an exit pressure in the vacuum expansion section of 1.20 Torr, which represents typical conditions in our experimental facility. We choose to study a case where 4 kW of microwave energy is added in the subsonic stage and the total mass flow rate is approximately 220 mg/sec, representing one possible operating point for the prototype thruster. These conditions correspond to a specific power of 18 MJ/kg, which falls into a range which was previously studied in experiments.[14]

Navier-Stokes Equations

The unsteady axisymmetric Navier-Stokes equations, for a two-temperature gas with reacting species can be written in cylindrical coordinates in the following differential vector form

$$\frac{\partial r\mathbf{U}}{\partial t} + \frac{\partial r\mathbf{F}(\mathbf{U})}{\partial x} + \frac{\partial r\mathbf{G}(\mathbf{U})}{\partial r} = \mathbf{S}, \qquad (1)$$

where x and r are the axial and radial directions, respectively. $\mathbf{U} = (\rho_i, \rho u, \rho v, E_h, E_e)^{\mathrm{T}}$ is the vector of conservation variables, where ρ_i represents the mass density of species i, ρ is the total mass density (neglecting the contribution due to the electron mass density, ρ_e), u is the axial velocity, and v the radial velocity. The total heavy particle energy density (thermal plus directed kinetic) is expressed as

$$E_h = \Sigma_h \rho_i \left(\frac{3}{2} R_i T + 1/2[u^2 + v^2] + \beta_i \right),$$

where β_i and R_i are the enthalpy of formation and the gas constant for species i, and T is the heavy particle temperature. The summation includes all the species except the electrons. The electron energy density is taken to be $E_e = (3/2)\rho_e R_e T_e$, where R_e is the electron gas constant and T_e the electron temperature. The flux vectors, $\mathbf{F}(\mathbf{U}) = \mathbf{F^c}(\mathbf{U}) - \mathbf{F^d}(\mathbf{U})$ and $\mathbf{G}(\mathbf{U}) = \mathbf{G^c}(\mathbf{U}) - \mathbf{G^d}(\mathbf{U})$, are functions of the conservation variables and contain both convective and diffusive terms, represented by the superscripts c and d respectively. The convective flux vectors are

$$\mathbf{F^c}(\mathbf{U}) = \begin{bmatrix} \rho_i u \\ \rho u^2 + P \\ \rho u v \\ u(E_h + P_h) \\ u(E_e + P_e) \end{bmatrix},$$

$$\mathbf{G^c}(\mathbf{U}) = \begin{bmatrix} \rho_i v \\ \rho u v \\ \rho v^2 + P \\ v(E_h + P_h) \\ v(E_e + P_e) \end{bmatrix},$$

while the diffusive flux vectors are

$$\mathbf{F^d}(\mathbf{U}) = \begin{bmatrix} 0 \\ \tau_{xx} \\ \tau_{xr} \\ -q_{hx} + u\tau_{xx} + v\tau_{xr} \\ -q_{ex} \end{bmatrix},$$

$$\mathbf{G^d}(\mathbf{U}) = \begin{bmatrix} 0 \\ \tau_{xr} \\ \tau_{rr} \\ -q_{hr} + u\tau_{xr} + v\tau_{rr} \\ -q_{er} \end{bmatrix},$$

where P is the total gas pressure, τ_{xx}, τ_{xr}, and τ_{rr} are the components of the gas stress tensor, q_{hx} and q_{hr} are the components of heavy particle heat flux and q_{ex} and q_{er} are the components of the electron heat flux. The heavy particle pressure is expressed as $P_h = \Sigma_h \rho_i R_i T$ and the electron pressure is $P_e = \rho_e R_e T_e$. The components of the heat fluxes and the stress tensor are related to temperature and velocity derivatives by the transport coefficients, μ, k_h, k_e, as described in previous work.[12] The method used to calculate the transport coefficients and the complex electrical conductivity, σ, are discussed in the transport properities section. Species mass diffusion is neglected in this work. The right hand side of Eqn. 1, $\mathbf{S}$, contains source terms that are due to the cylindrical symmetry of the problem, the finite rate of electronic excitation and ionization reactions, the energy transfer between electrons and heavy particles, and microwave joule heating

rate, Q_J. The source term is given below

$$\mathbf{S} = \begin{bmatrix} r\Omega_i \\ p + \frac{2}{3}\left(\tau_{xr} - \frac{2\mu v}{r}\right) \\ r(Q_e + Q_{in}) \\ r(-Q_e - Q_{in} + Q_J) \end{bmatrix}.$$

In the above expression Ω_i is the rate of mass production for species i due to ionization and electronic excitation processes. The microwave joule heating rate is a function of the complex electric field amplitudes E_r and E_z according to the following formula

$$Q_J = \frac{1}{4}\left(\sigma + \sigma^*\right)\left(E_r E_r^* + E_z E_z^*\right). \qquad (2)$$

The energy transfer from electrons to heavy particles due to elastic collisions is Q_e and the inelastic energy transfer term is Q_{in}. Q_e is determined in the same way as in the previous work,[12] but using a more accurate expression for the energy-averaged elastic collision frequency of electrons with helium atoms

$$\nu_{ea} = 1.45310^{-15} N_{He} Te^{0.381}.$$

This expression was obtained by numerically integrating experimental data for the elastic scattering cross section.[16] The inelastic energy transfer term is the sum of all net ionization and excitation reaction rates weighted by the individual reaction energies, $\Delta\epsilon_{ij}$. The chemical source term, Ω_i, for each of the species in the model, is discussed in the collisional reaction rates section.

A conservative finite-volume numerical discretization, incorporating first-order scalar dissipation, is used to integrate the governing equations(1) in time until a steady state is reached, an approach that has been thoroughly validated by several authors.[17–19] We use an explict time integration scheme. In the work previously mentioned, involving high speed supersonic flows, the criteria for judging when a solution was properly converged was the reduction of the density residual by at least five orders of magnitude. This criterion has worked well in the past and therefore we will adopt it here, however it should be noted that an unambiguous measure of convergence is when all the residuals, not just the density residual, have decreased by many orders of magnitude. In this work the time step is determined individually for each cell on the grid

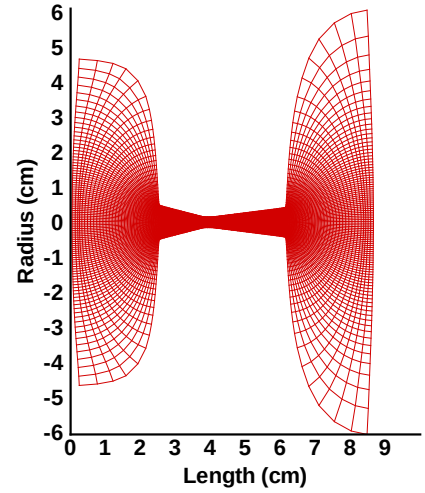

Fig. 2 The structured grid generated for the thruster geometry. The grid points have been reflected about the axis of symmetry axis (x axis).

and the electron and heavy species equations are advanced with their own characteristic time step size. This last point is essential, because the addition of an electron energy equation adds stiffness to the problem. A structured grid was used for all the simulations in this work, consisting of 49 radial cells and 105 axial cells, as shown in Figure 2. These grid points where generated by solving the Laplace equation to find the streamlines and the lines of constant velocity potential for the geometry of the prototype thruster. A finite-element routine, similar to those used for finding the microwave field components and for calculating the heat transfer at the nozzle wall, was used for this purpose.

Collisional Reaction Rates

We consider three distinct types of collisional processes when calculating the individual species mass density source terms, Ω_i. These processes are listed below, followed by a brief discussion of how the rate cofficients are determined for each case.

(a) Excitation and de-excitation by electron collisions

$$\mathrm{He}(i) + e^- \underset{\beta_k}{\overset{S_k}{\rightleftarrows}} \mathrm{He}(j) + e^-.$$

We include seven of these reactions for the following pairs of species, (i,j):

$(1\,^1S,2\,^1S)$,$(1\,^1S,2\,^3S)$,$(2\,^1S,2\,^1P)$,$(2\,^1S,2\,^3P)$, $(2\,^3S,2\,^1S)$,$(2\,^3S,2\,^1P)$,$(2\,^3S,2\,^3P)$.

(b) Ionization by electron impact and three-body recombination

$$\mathrm{He}(i) + e^- \underset{\beta_k}{\overset{S_k}{\rightleftarrows}} \mathrm{He}^+ + 2e^-.$$

The index i includes all excited species and the ground state.

(c) Penning ionization

$$\begin{aligned} \mathrm{He}(i) + \mathrm{He}(j) \quad & \overset{x\beta}{\rightarrow} \quad \mathrm{He}(1\,^1S) + \mathrm{He}^+ + e^- \\ & \overset{(1-x)\beta}{\rightarrow} \quad \mathrm{He}_2^+ + e^-. \end{aligned}$$

Six Penning reactions are considered in this paper, including reactions involving the following pairs of excited species, (i,j): $(2\ \ ^1S,2\ \ ^1S)$,$(2\ \ ^1S,2\ \ ^3S)$,$(2\ \ ^1S,2\ \ ^3P)$, $(2\,^3S,2\,^3S)$,$(2\,^3S,2\,^3P)$,$(2\,^3P,2\,^3P)$.

For the electron collision processes considered above, S_k is the ionization or electronic excitation rate constant, respectively, for reaction k, involving species i and j, and β_k is the corresponding three-body recombination or de-excitation rate constant. All together twelve ionization and excitation reactions were considered in this work. The forward rate constant for reaction k, S_k, is obtained by integrating the appropriate cross sections over a Maxwellian electron energy distribution for different values of electron temperature. The corresponding Arrehenius coefficients, A_k and n_k are then determined by fitting the results to the following formula

$$S_k = A_k T_e^{n_k} \exp \frac{-\Delta\epsilon_{ij}}{kTe}$$

The cross-sections for the above processes were taken from a compilation of experimental data for He given in Ref. 18, and the numerical integration was performed using Guassian quadratures. The backward rate constants for He, β_k, were determined using the forward rate constants and the Klein-Rosenland relations. The rate constants β and X for Penning ionization were taken from Ref. 18.

Transport Properties

In our model we consider both heavy particle and electron transport processes. For the heavy particles viscosity and thermal conductivity are calculated, and for the electrons thermal and electrical conductivity are calculated. For pure helium the viscosity and thermal conductivity are taken from the results of kinetic theory for a monatomic gas,[20]

$$\begin{aligned} \mu_{He} &= \frac{5\sqrt{\pi m_{He} kT}}{16\pi\Omega^{(2,2)}} \\ k_{He} &= \frac{25\sqrt{\pi m_{He} kT}\, c_v}{32\pi\Omega^{(2,2)}}, \end{aligned}$$

where $\Omega^{(2,2)}$ is a collision integral, evaluated assuming a Lennard-Jones potential, and c_v is the specific heat of helium. For pure helium ions, either He^+ or He_2^+, the corresponding expressions are[21]

$$\begin{aligned} \mu_i &= 0.72 \frac{\sqrt{m_i}\,(4\pi\epsilon_0)^2\,(kT)^{5/2}}{\sqrt{\pi} e^4 \Lambda} \\ k_i &= 2.925 \frac{k\,(4\pi\epsilon_0)^2\,(kT)^{5/2}}{\sqrt{\pi m_i} e^4 \Lambda}, \end{aligned}$$

where Λ is the Coulomb logorithm and m_i is the mass of the ion. The viscosity, μ_h, and thermal conductivity, k_h, of the mixture are both determined from the pure atom and ion values using the same empirical mixture rule.[22]

The electron thermal conductivity, k_e, is calculated using the Frost mixture rule formula,[21] involving the following integration of the electron energy distribution

$$k_e = \frac{4N_e k^2 T_e}{3\sqrt{\pi} m_e} \int_0^\infty \frac{[X - 5/2]^2\, X^{3/2} \exp -X}{\nu_k} dX,$$

where ν_k is an electron collision frequency term, including contributions from both electron-neutral and Coulomb collisions. The electron energy has been non-dimensionalized by kT_e in this integral. A similar Frost mixture rule formula is used for calculating the complex electrical conductivity[21]

$$\sigma = \frac{4N_e e^2}{3\sqrt{\pi} m_e} \int_0^\infty \frac{X^{3/2} \exp -X}{\nu_c + i\omega} dX,$$

where ν_c is another electron collision frequency term, different from ν_k, and ω is the angular frequency of the microwave field. These integrals are solved in our numerical simulations by using a ten point Gauss-Laguerre formula.

Nozzle Heat Transfer

Heat transfer through the nozzle wall is considered in our model. We solve for the temperature distribution inside the nozzle, section E in Fig. 1, and then compute the heat transfer normal to the wall for use by the fluid solver. The temperature distribution inside the nozzle is given by the solution of the following equation

$$\frac{1}{r}\frac{\partial}{\partial r}r\frac{\partial T}{\partial r}+\frac{\partial^2 T}{\partial x^2}=0.$$

In solving this equation we assume that the temperature on the outside surface of the nozzle is 300 K; the temperature on the inside surface is supplied by the fluid solver. A finite-element solver, similar to those used to solve for the microwave field components, is used to solve this equation. The nozzle heat transfer rate is recalculated after 50 time steps of the fluid solver. This completes the discussion of the equations that constitute the physical model.

Boundary Conditions

In this section the relevant boundary conditions for the fluid equations above are reviewed, the boundary conditions for the microwave field components are the same as in the previous work.[12,13] Because of the cell-centered scheme used by the Navier-Stokes solver it is necessary to specify the values of the flux vectors, $\mathbf{F}(\mathbf{U})$ and $\mathbf{G}(\mathbf{U})$, at the physical boundaries of the domain. Along the wall and centerline boundaries the convective fluxes are specified so that there are no mass, momentum or energy fluxes through these respective boundaries. In addition to the above specifications for the convective fluxes, the no slip conditions, $u = 0$ and $v = 0$, are applied at the wall boundary, this facilitates the computation of the diffusive fluxes, $\mathbf{F^d}(\mathbf{U})$ and $\mathbf{G^d}(\mathbf{U})$, at these locations. In addition the electrons are assumed to be adiabatic at the wall. The diffusive fluxes are zero at the gas inlet and exit planes. When calculating the convective fluxes at the inlet the stagnation conditions to the left of the boundary are specified, as mentioned before, and the flow velocity is extrapolated from the interior domain, to the right of the inlet. This is necessary in order to insure that the correct mass flow rate enters the domain in order for the flow to be choked at the throat. At the exit boundary in section D of Fig. 1, we calculate the convective fluxes in one of two ways, depending on whether the flow there is subsonic or supersonic. If the flow is supersonic the convective fluxes are calculated by extrapolating the flow properties from the interior of the domain to the left of the boundary. If the flow is subsonic we calculate the convective fluxes by specifying the pressure and temperature to be 1.20 Torr and 500 K, and extrapolating the velocity from the flow interior. Cylindrical symmetry is enforced along the centerline, by setting v and all partial derivatives with respect to r equal to zero.

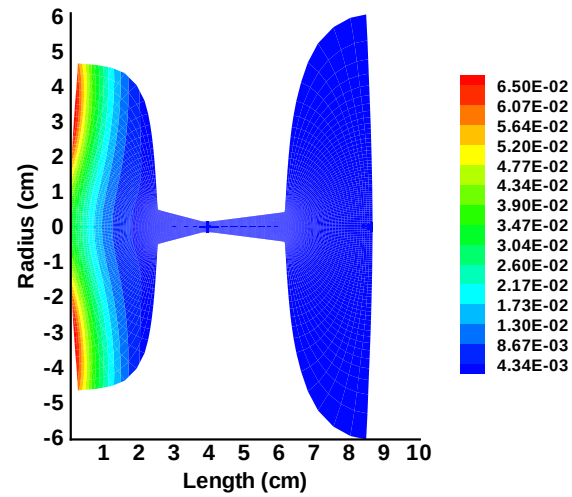

Fig. 3 Joule heating rate of electrons inside the microwave thruster(in kW/cm^3).

Simulation Results

The results of a simulation involving 4 kW of subsonic energy addition are now presented, starting first with Q_J contours, as shown in Fig. 3. The maximum joule heating rate of 0.0694 kW/cm^3 is not located on the centerline, but occurs a distance of approximately 3.157 cm above the centerline in a region adjacent to the inlet, at $x = 0.142$ cm. The temperature and electron temperature at this point are 2,110 K and 15,100 K, respectively as shown in Fig. 4 and Fig. 5. The cooresponding values on the centerline are lower than these, 1,260 K and 7,820 K. It is readily

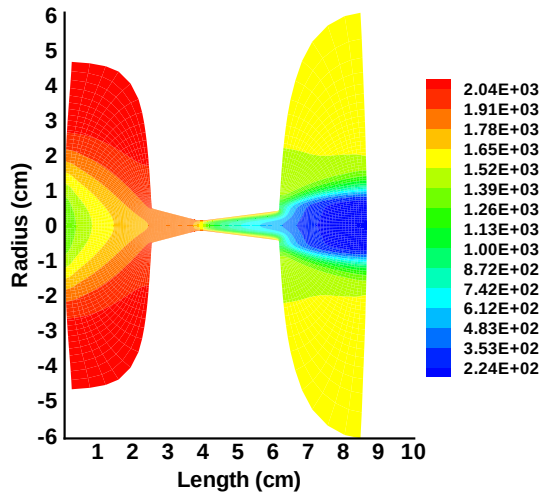

Fig. 4 Gas temperature contours inside the microwave thruster (in K), without supersonic energy addition.

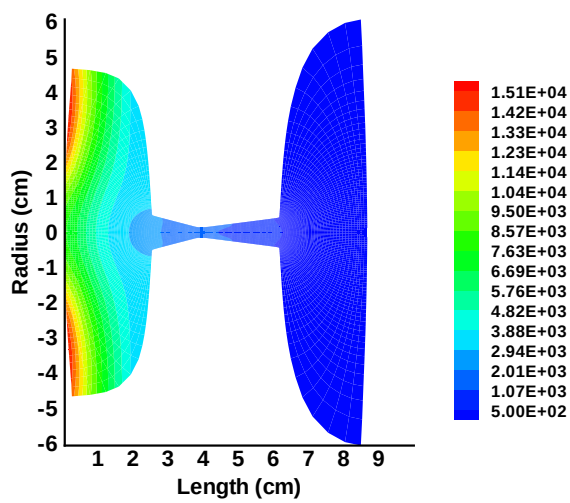

Fig. 5 Electron temperature contours inside the microwave thruster (in K), without supersonic energy addition.

apparent that the electron temperature profile is markedly different than the gas temperature profile, by an order of magnitude. The disparity between the electron and heavy species temperature occurs, even though the gas pressure is as high as 861 Torr at the point of maximum joule heating. The total pressure contours, in Torr, are shown in Fig. 6. The pressure is relatively constant in the subsonic plenum section (860 Torr), as one would expect.

For microwaves at 2.45 GHz the critical electron number density is $7.45 \times 10^{10}\text{cm}^{-3}$. The

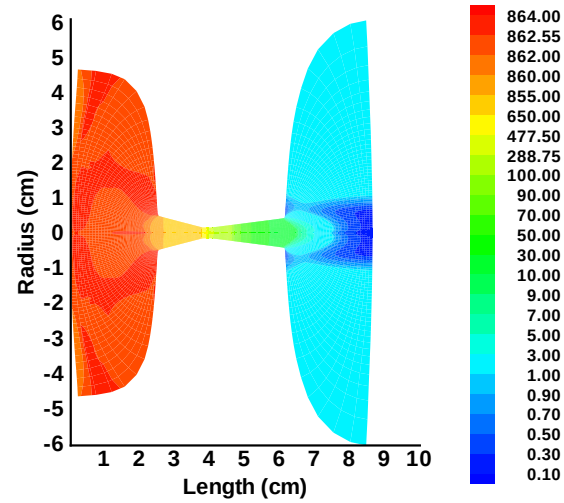

Fig. 6 Pressure contours inside the microwave thruster (in Torr), without supersonic energy addition.

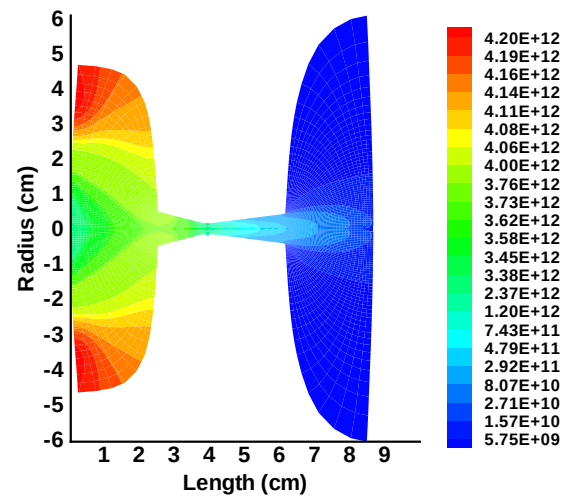

Fig. 7 Electron number density contours inside the microwave thruster(in cm^{-3}).

electron number density in this problem is larger than this, as shown in Fig. 7. The maximum electron number density is $4.21 \times 10^{12}\text{cm}^{-3}$, which occurs at the point slightly above the point of maximum joule heating rate, at $y = 3.70$ cm above the centerline. The electron number density drops to $3.14 \times 10^{12}\text{cm}^{-3}$ at the centerline, which illustrates once more the annular nature of the energy addition profile. The number densities of the $2\ ^1S$ and $2\ ^3S$ helium metastable states at point of maximum joule heating are 4.53×10^{10} and $3.93 \times 10^{10}\text{cm}^{-3}$, as shown in Fig. 8 and Fig. 9. Taking the electron temperature value just men-

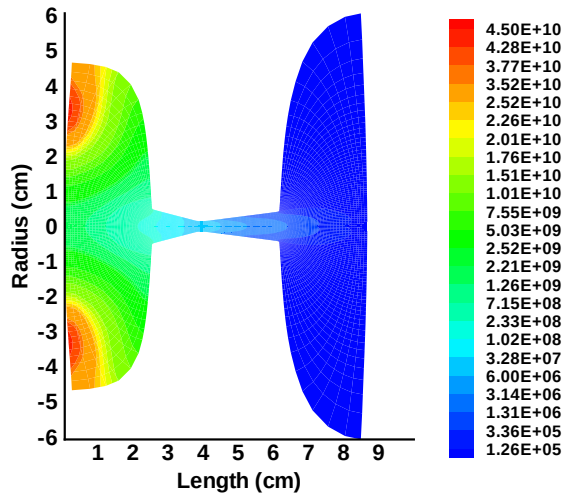

Fig. 8 $2\ ^1S$ **number density contours inside the microwave thruster(in cm^{-3}).**

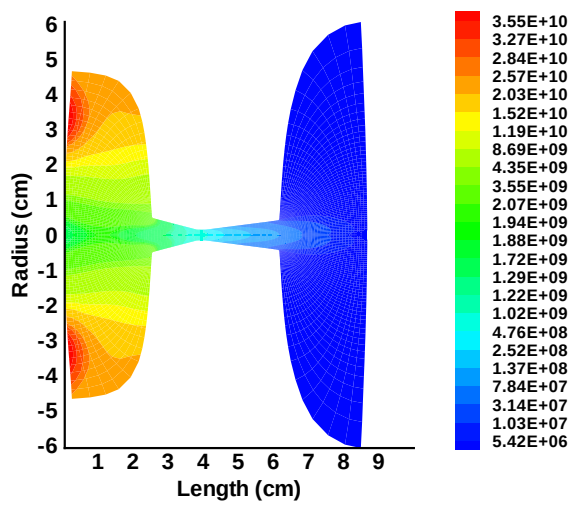

Fig. 9 $2\ ^3S$ **number density contours inside the microwave thruster(in cm^{-3}).**

tioned at this point, and the ground state number density, which is $3.91 \times 10^{18}\text{cm}^{-3}$, we can calculate what the number densities of these species should be, if a Boltzmann equilibrium is maintained among the different excited states. We find these numbers to be $3.2 \times 10^{11}\text{cm}^{-3}$ for $2\ ^1S$ and $1.80 \times 10^{12}\text{cm}^{-3}$ for $2\ ^3S$; in both cases, therefore, the metastable number density differs from the Boltzmann equilibrium value by more than an order of magnitude, a clear example of why the inclusion of finite rate kinetics for ionization and excitation in the model is essential. The metastable number densities at the throat, on

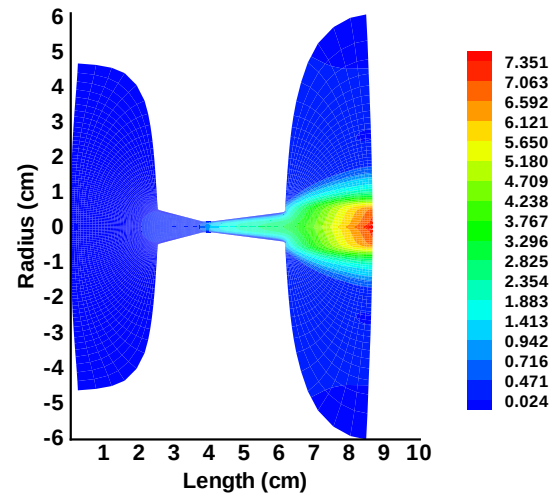

Fig. 10 Mach number contours inside the microwave thruster.

the centerline, are $1.35 \times 10^7\text{cm}^{-3}$ for $2\ ^1S$ and $5.51 \times 10^8\text{cm}^{-3}$ for $2\ ^3S$, where the gas pressure is 369 Torr. The electron number density at this point is $2.08 \times 10^{12}\text{cm}^{-3}$.

The Mach number contours inside the thruster are shown in Fig. 10. Without supersonic energy addition the Mach number on the centerline at the nozzle exit is 2.97. The flow is underexpanded at the nozzle exit, since the exit pressure is about 15.6 Torr and the background pressure in the vacuum expansion region is roughly 1.20 Torr; the expansion fans at the nozzle exit can be seen in Fig. 4 and Fig. 6. The axial velocity contours are shown in Fig. 11. The axial velocity at the exit, on the centerline, is about 3.80 km/sec.

For the case considered, with 4 kW energy addition in the plenum and no supersonic energy addition, the thrust of this microwave thruster is 0.721 N, for 220 mg/sec mass flow rate, and the specific impulse is 334 sec. The results of this calculation show that of the power absorbed in the plenum, 21 W is transferred to the nozzle wall section due to thermal conduction of the heavy particles; this fact by itself would seem to suggest that the enthalpy transfered to the gas by the plasma is converted to thrust in an efficient manner. The total energy flux exiting the nozzle, however, is only 2890 W. An additional energy flux of 1100 W flows out of the thruster domain through the plenum side, as explained in the discussion section. The difference between the sum of these two energy fluxes and the total microwave

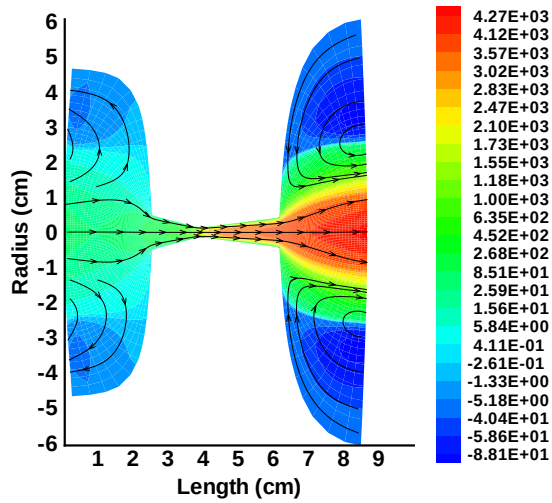

Fig. 11 Axial velocity contours inside the microwave thruster(in m/sec). A few streamlines are shown in the figure to indicate the direction of the flow.

input power is only about 10 W, a strong indication that the calculation has achieved a sufficient level of convergence to model steady state conditions.

Discussion

Unlike the previous results with a supersonic helium flow, where only ionization from the ground state was considered and the resulting maximum electron temperature was 40,000 K, in this work, where we include 12 differrent, electron impact ionization and excitation processes, we find a significantly reduced electron temperature which varies from roughly 15,100 K at the point of maximum energy addition to 2,390 K, just before the converging section of the nozzle. The current result for the peak electron temperature agrees well with spectroscopic measurements of the electron temperature in microwave helium discharges cited above; in that work the electron temperature was found to be 12,000 K. Unlike the plasmas observed in experiments with similar values of specific power (18 MJ/kg),[14] we find in our calculations that the plasma is not concentrated on the centerline, with the point of maximum electron temperature and number density being at least 3.157 cm above the axis. Experimentally little radial variation in electron temperature was observed, and our results support this as seen by inspecting the contours in Fig. 5. However experiments show that the peak temperature was on the centerline, and this is not the case with our simulation results. One possible reason for this discrepancy is that we do not include an azimuthal velocity component in our model, and several of the experimental studies cited in this paper have stressed the importance of using a stabilization device such as a flow swirler or a bluff body, which induces azimuthal velocity in the flow, to help maintain a stable plasma. Whether the absence of azimuthal velocity in the model leads to our result of voluminous plasma with the maximum joule heating occurring in an annular region is a topic for future investigation.

One point is clear, as in the previous work with the two-stage thruster, here we see once again the importance of including separate electron temperature and heavy particle temperatures, even at relatively high pressure of more than one atmosphere in the plenum. Any model that describes this kind of microwave heating problem must include a separate electron energy equation.

Another point to address is the issue as to why the fluid energy flux at the nozzle exit is not the same as the microwave input power. By looking at the velocity streamlines in the plenum section, shown in Fig. 11, we see that there is in fact evidence of a recirculation zone in the plenum, with some streamlines moving from right to left across the inlet boundary. In these regions energy is carried out of the domain, and there is no way for this energy to be transported back into the thruster and contribute to the calculated thrust. Perhaps the addition of azimuthal velocity to the model, may help to elminate this recirculation effect in the plenum.

Unlike previous models for microwave electrothermal thrusters which neglect one or more critical non-equilibrium processes, the model presented here incorporates many of these processes in a self-consistant manner and has already provided some insight into the highly non-equilibrium nature of the energy addition in this kind of thruster. Once additional work is done to validate the model, we can use this unique tool to accurately describe the performance of our two-stage prototype thruster and to explore the physics of new microwave thruster configurations as well.

Conclusions

A fully coupled calculation, solving both the Navier-Stokes and Maxwell equations has been performed for a microwave thruster. A case has been considered for helium propellant where 4 kW is deposited in the plenum. We can summarize our findings as follows:

- The plasma is highly non-equilibrium in nature, such that the electron and heavy particle temperature differ considerably and the number densities of helium metastable species are not in Boltzmann equilibrium.
- The peak electron temperature of 15,100 K is in good agreement with the experimentally observed value of 12,000 K.
- We observe a weak radial dependence of the electron temperature in the discharge region. This is also observed in experiments.
- The regions of maximum joule heating, electron temperature and number density occur in an annular region, more than 3.157 cm above the centerline. Experiments show that the maximum electron temperature occurs on the centerline.

Now that a fairly complete model, incorporating a body-fitted, structured grid and including the effects of separate electron and heavy species temperatures, non-equbilibrium ionization and excitation kinetics and nozzle heat transfer, has been applied to simulate a microwave thruster, several tasks remain in exploring the physics of this thruster. The next step is to do additional simulations and compare the results with thrust data for existing microwave thrusters. This will help to further validate the model.

References

[1]R.G. Jahn. *Physics of Electric Propulsion.* McGraw-Hill, 1968.

[2]P. G. Lichon and J. M. Sankovic. Development and demonstartion of a 600-sec mission-average i_{sp} arcjet. *Journal of Propulsion and Power*, 12:1018–1025, 1996.

[3]D.J. Sullivan. *Development and Performance Characterization of a Microwave Electrothermal Thruster Prototype.* PhD thesis, Pennsylvania State University, 1995.

[4]S. Whitehair and J. Asmussen. Microwave electrothermal thruster performance in helium gas. *Journal of Propulsion and Power*, 3:136–144, 1985.

[5]D. J. Sullivan and M. M. Micci. Development of a microwave resonant cavity electrothermal thruster prototype. In 23rd *International Electric Propulsion Conference*, Seattle, WA, September 1993. IEPC-93-036.

[6]S. Venkateswaran and C. L. Merkle. Numerical investigation of bluff-body stabilized microwave plasams. *Journal of Propulsion and Power*, 11:357–364, 1995.

[7]D.A. Schwer, S. Venkateswaran, and C. L. Merkle. Analysis of microwave-heated rocket engines for space propulsion. In *AIAA* 29th *Joint Propulsion Conference*, Monterey, CA, June 1993. AIAA 93-2105.

[8]S. A. Miller and M. Martinez-Sanchez. Two-fluid nonequilibrium simulation of hydrogen arcjet thrusters. *Journal of Propulsion and Power*, 12:112–119, 1996.

[9]T. W. Megli, H. Krier, R. L. Burton, and A. Mertogul. Two-temperature plasma modeling of nitrogen/hydrogen arcjets. *Journal of Propulsion and Power*, 12:1062–1069, 1996.

[10]J. Heiermann and M. Auweter-Kurtz. Numerical and experimental investigation of the current distribution in self-field mpd thrusters. In 37rd *AIAA Joint Propulsion Conference*, Salt Lake City, UT, July 2001. AIAA-2001-3498.

[11]K. Sankaran, S. C. Jardin, and E. Y. Choueiri. Application of a new numerical solver to the simulation of mpd flows. In 36rd *AIAA Joint Propulsion Conference*, Huntsville, AL, July 2000. AIAA-2000-3537.

[12]V. P. Chiravalle, R. B. Miles, and E. Y. Choueiri. Nonequilibrium numerical study of a two-stage microwave electrothermal thruster. In 27rd *International Electric Propulsion Conference*, Pasadena, CA, October 2001. IEPC-2001-194.

[13]V. P. Chiravalle, R. B. Miles, and E. Y. Choueiri. Numerical simulation of microwave-sustained supersonic plasmas for application to space propulsion. In 39rd *AIAA Aerospace Sciences Meeting*, Reno, NV, January 2001. AIAA-2001-0962.

[14]P. Balaam and M. M. Micci. Investigation of stabilized resonant cavity microwave plasmas for propulsion. *Journal of Propulsion and Power*, 11:1021–1027, 1995.

[15]D.R. Lide. *Handbook of Chemistry and Physics.* CRC Press, 2000.

[16]R.W. Crompton, M.T. Elford, and R.L. Jory. The momentum transfer cross section for electrons in helium. *Australian Journal of Physics*, 20:369–400, 1967.

[17]R. Broglia, M. Manna, H. Deconinck, and G. Degrez. Development and validation of an axisymmetric navier-stokes solver for hypersonic flows. Technical Note 188, von Karman Institute for Fluid Dynamics, 1995.

[18]L. Martinelli. *Calculations of Viscous Flows with a Multigrid Method.* PhD thesis, Princeton University, 1987.

[19]G.L. Brown, A.P. Ratta, R.W. Anderson, L. Martinelli, W.R. Lempert, and R.B. Miles. Fluid mechanics in a radiatively driven hypseronic wind-tunnel - prediction and preliminary experiment. In 19rd *AIAA Advanced Measurement and Ground Testing Technology Conference*, New Orleans, LA, June 1996. AIAA-96-2199.

[20]J.O. Hirshfelder, C.F. Curtiss, and R.B. Bird. *Molecular Theory of Gases and Liquids.* John Wiley & Sons, 1954.

[21]M. Mitchner and C. H. Kruger. *Partially Ionized Gases*. John Wiley & Sons, 1973.

[22]R.B. Bird, W.E. Stewart, and E.N. Lightfoot. *Transport Phenomena*. John Wiley & Sons, 1960.